

Measurement of the muon charge asymmetry from W boson decays

V.M. Abazov³⁵, B. Abbott⁷⁵, M. Abolins⁶⁵, B.S. Acharya²⁸, M. Adams⁵¹, T. Adams⁴⁹, E. Aguilo⁵, S.H. Ahn³⁰, M. Ahsan⁵⁹, G.D. Alexeev³⁵, G. Alkhazov³⁹, A. Alton^{64,a}, G. Alverson⁶³, G.A. Alves², M. Anastasoie³⁴, L.S. Ancu³⁴, T. Andeen⁵³, S. Anderson⁴⁵, B. Andrieu¹⁶, M.S. Anzels⁵³, Y. Arnaud¹³, M. Arov⁶⁰, M. Arthaud¹⁷, A. Askew⁴⁹, B. Åsman⁴⁰, A.C.S. Assis Jesus³, O. Atramentov⁴⁹, C. Autermann²⁰, C. Avila⁷, C. Ay²³, F. Badaud¹², A. Baden⁶¹, L. Bagby⁵², B. Baldin⁵⁰, D.V. Bandurin⁵⁹, S. Banerjee²⁸, P. Banerjee²⁸, E. Barberis⁶³, A.-F. Barfuss¹⁴, P. Bargassa⁸⁰, P. Baringer⁵⁸, J. Barreto², J.F. Bartlett⁵⁰, U. Bassler¹⁶, D. Bauer⁴³, S. Beale⁵, A. Bean⁵⁸, M. Begalli³, M. Begel⁷¹, C. Belanger-Champagne⁴⁰, L. Bellantoni⁵⁰, A. Bellavance⁵⁰, J.A. Benitez⁶⁵, S.B. Beri²⁶, G. Bernardi¹⁶, R. Bernhard²², L. Berntzon¹⁴, I. Bertram⁴², M. Besançon¹⁷, R. Beuselinck⁴³, V.A. Bezzubov³⁸, P.C. Bhat⁵⁰, V. Bhatnagar²⁶, C. Biscarat¹⁹, G. Blazey⁵², F. Blekman⁴³, S. Blessing⁴⁹, D. Bloch¹⁸, K. Bloom⁶⁷, A. Boehnlein⁵⁰, D. Boline⁶², T.A. Bolton⁵⁹, G. Borissov⁴², T. Bose⁷⁷, A. Brandt⁷⁸, R. Brock⁶⁵, G. Brooijmans⁷⁰, A. Bross⁵⁰, D. Brown⁸¹, N.J. Buchanan⁴⁹, D. Buchholz⁵³, M. Buehler⁸¹, V. Buescher²¹, S. Bunichev³⁷, S. Burdin^{42,b}, S. Burke⁴⁵, T.H. Burnett⁸², C.P. Buszello⁴³, J.M. Butler⁶², P. Calfayan²⁴, S. Calvet¹⁴, J. Cammin⁷¹, W. Carvalho³, B.C.K. Casey⁷⁷, N.M. Cason⁵⁵, H. Castilla-Valdez³², S. Chakrabarti¹⁷, D. Chakraborty⁵², K.M. Chan⁵⁵, K. Chan⁵, A. Chandra⁴⁸, F. Charles^{18,†}, E. Cheu⁴⁵, F. Chevallier¹³, D.K. Cho⁶², S. Choi³¹, B. Choudhary²⁷, L. Christofek⁷⁷, T. Christoudias^{43,†}, S. Cihangir⁵⁰, D. Claes⁶⁷, B. Clément¹⁸, Y. Coadou⁵, M. Cooke⁸⁰, W.E. Cooper⁵⁰, M. Corcoran⁸⁰, F. Couderc¹⁷, M.-C. Cousinou¹⁴, S. Crépe-Renaudin¹³, D. Cutts⁷⁷, M. Ćwiok²⁹, H. da Motta², A. Das⁶², G. Davies⁴³, K. De⁷⁸, S.J. de Jong³⁴, E. De La Cruz-Burelo⁶⁴, C. De Oliveira Martins³, J.D. Degenhardt⁶⁴, F. Déliot¹⁷, M. Demarteau⁵⁰, R. Demina⁷¹, D. Denisov⁵⁰, S.P. Denisov³⁸, S. Desai⁵⁰, H.T. Diehl⁵⁰, M. Diesburg⁵⁰, A. Dominguez⁶⁷, H. Dong⁷², L.V. Dudko³⁷, L. Dufloc¹⁵, S.R. Dugad²⁸, D. Duggan⁴⁹, A. Duperrin¹⁴, J. Dyer⁶⁵, A. Dyshkant⁵², M. Eads⁶⁷, D. Edmunds⁶⁵, J. Ellison⁴⁸, V.D. Elvira⁵⁰, Y. Enari⁷⁷, S. Eno⁶¹, P. Ermolov³⁷, H. Evans⁵⁴, A. Evdokimov⁷³, V.N. Evdokimov³⁸, A.V. Ferapontov⁵⁹, T. Ferbel⁷¹, F. Fiedler²⁴, F. Filthaut³⁴, W. Fisher⁵⁰, H.E. Fisk⁵⁰, M. Ford⁴⁴, M. Fortner⁵², H. Fox²², S. Fu⁵⁰, S. Fuess⁵⁰, T. Gadfort⁸², C.F. Galea³⁴, E. Gallas⁵⁰, E. Galyaev⁵⁵, C. Garcia⁷¹, A. Garcia-Bellido⁸², V. Gavrilov³⁶, P. Gay¹², W. Geist¹⁸, D. Gelé¹⁸, C.E. Gerber⁵¹, Y. Gershtein⁴⁹, D. Gillberg⁵, G. Ginter⁷¹, N. Gollub⁴⁰, B. Gómez⁷, A. Goussiou⁵⁵, P.D. Grannis⁷², H. Greenlee⁵⁰, Z.D. Greenwood⁶⁰, E.M. Gregores⁴, G. Grenier¹⁹, Ph. Gris¹², J.-F. Grivaz¹⁵, A. Grohsjean²⁴, S. Grünendahl⁵⁰, M.W. Grünewald²⁹, J. Guo⁷², F. Guo⁷², P. Gutierrez⁷⁵, G. Gutierrez⁵⁰, A. Haas⁷⁰, N.J. Hadley⁶¹, P. Haefner²⁴, S. Hagopian⁴⁹, J. Haley⁶⁸, I. Hall⁶⁵, R.E. Hall⁴⁷, L. Han⁶, K. Hanagaki⁵⁰, P. Hansson⁴⁰, K. Harder⁴⁴, A. Harel⁷¹, R. Harrington⁶³, J.M. Hauptman⁵⁷, R. Hauser⁶⁵, J. Hays⁴³, T. Hebbeker²⁰, D. Hedin⁵², J.G. Hegeman³³, J.M. Heinmiller⁵¹, A.P. Heinson⁴⁸, U. Heintz⁶², C. Hensel⁵⁸, K. Herner⁷², G. Hesketh⁶³, M.D. Hildreth⁵⁵, R. Hirosky⁸¹, J.D. Hobbs⁷², B. Hoeneisen¹¹, H. Hoeth²⁵, M. Hohlfeld²¹, S.J. Hong³⁰, S. Hossain⁷⁵, P. Houben³³, Y. Hu⁷², Z. Hubacek⁹, V. Hynek⁸, I. Iashvili⁶⁹, R. Illingworth⁵⁰, A.S. Ito⁵⁰, S. Jabeen⁶², M. Jaffré¹⁵, S. Jain⁷⁵, K. Jakobs²², C. Jarvis⁶¹, R. Jesik⁴³, K. Johns⁴⁵, C. Johnson⁷⁰, M. Johnson⁵⁰, A. Jonckheere⁵⁰, P. Jonsson⁴³, A. Juste⁵⁰, D. Käfer²⁰, S. Kahn⁷³, E. Kajfasz¹⁴, A.M. Kalinin³⁵, J.R. Kalk⁶⁵, J.M. Kalk⁶⁰, S. Kappler²⁰, D. Karmanov³⁷, J. Kasper⁶², P. Kasper⁵⁰, I. Katsanos⁷⁰, D. Kau⁴⁹, R. Kaur²⁶, V. Kaushik⁷⁸, R. Kehoe⁷⁹, S. Kermiche¹⁴, N. Khalatyan³⁸, A. Khanov⁷⁶, A. Kharchilava⁶⁹, Y.M. Kharzheev³⁵, D. Khatidze⁷⁰, H. Kim³¹, T.J. Kim³⁰, M.H. Kirby³⁴, M. Kirsch²⁰, B. Klima⁵⁰, J.M. Kohli²⁶, J.-P. Konrath²², M. Kopal⁷⁵, V.M. Korablev³⁸, A.V. Kozelov³⁸, D. Krop⁵⁴, T. Kuhl²³, A. Kumar⁶⁹, S. Kunori⁶¹, A. Kupco¹⁰, T. Kurča¹⁹, J. Kvita⁸, F. Lacroix¹², D. Lam⁵⁵, S. Lammers⁷⁰, G. Landsberg⁷⁷, P. Lebrun¹⁹, W.M. Lee⁵⁰, A. Leflat³⁷, F. Lehner⁴¹, J. Lellouch¹⁶, J. Leveque⁴⁵, P. Lewis⁴³, J. Li⁷⁸, Q.Z. Li⁵⁰, L. Li⁴⁸, S.M. Lietti⁴, J.G.R. Lima⁵², D. Lincoln⁵⁰, J. Linnemann⁶⁵, V.V. Lipaev³⁸, R. Lipton⁵⁰, Y. Liu^{6,†}, Z. Liu⁵, L. Lobo⁴³, A. Lobodenko³⁹, M. Lokajicek¹⁰, A. Lounis¹⁸, P. Love⁴², H.J. Lubatti⁸², A.L. Lyon⁵⁰, A.K.A. Maciel², D. Mackin⁸⁰, R.J. Madaras⁴⁶, P. Mättig²⁵, C. Magass²⁰, A. Magerkurth⁶⁴, N. Makovec¹⁵, P.K. Mal⁵⁵, H.B. Malbouisson³, S. Malik⁶⁷, V.L. Malyshev³⁵, H.S. Mao⁵⁰, Y. Maravin⁵⁹, B. Martin¹³, R. McCarthy⁷², A. Melnitchouk⁶⁶, A. Mendes¹⁴, L. Mendoza⁷, P.G. Mercadante⁴, M. Merkin³⁷, K.W. Merritt⁵⁰, J. Meyer²¹, A. Meyer²⁰, M. Michaut¹⁷, T. Millet¹⁹, J. Mitrevski⁷⁰, J. Molina³, R.K. Mommsen⁴⁴, N.K. Mondal²⁸, R.W. Moore⁵, T. Moulík⁵⁸, G.S. Muanza¹⁹, M. Mulders⁵⁰, M. Mulhearn⁷⁰, O. Mundal²¹, L. Mundim³, E. Nagy¹⁴, M. Naimuddin⁵⁰, M. Narain⁷⁷, N.A. Naumann³⁴, H.A. Neal⁶⁴, J.P. Negret⁷, P. Neustroev³⁹, H. Nilsen²², H. Nogima³, A. Nomerotski⁵⁰, S.F. Novaes⁴, T. Nunnemann²⁴, V. O'Dell⁵⁰, D.C. O'Neil⁵, G. Obrant³⁹, C. Ochando¹⁵, D. Onoprienko⁵⁹, N. Oshima⁵⁰, J. Osta⁵⁵, R. Otec⁹, G.J. Otero y Garzón⁵¹, M. Owen⁴⁴, P. Padley⁸⁰, M. Pangilinan⁷⁷, N. Parashar⁵⁶, S.-J. Park⁷¹, S.K. Park³⁰, J. Parsons⁷⁰, R. Partridge⁷⁷, N. Parua⁵⁴,

A. Patwa⁷³, G. Pawloski⁸⁰, B. Penning²², M. Perfilov³⁷, K. Peters⁴⁴, Y. Peters²⁵, P. Pétroff¹⁵, M. Petteni⁴³, R. Piegaia¹, J. Piper⁶⁵, M.-A. Pleier²¹, P.L.M. Podesta-Lerma^{32,c}, V.M. Podstavkov⁵⁰, Y. Pogorelov⁵⁵, M.-E. Pol², P. Polozov³⁶, B.G. Pope⁶⁵, A.V. Popov³⁸, C. Potter⁵, W.L. Prado da Silva³, H.B. Prosper⁴⁹, S. Protopopescu⁷³, J. Qian⁶⁴, A. Quadt^{21,d}, B. Quinn⁶⁶, A. Rakitine⁴², M.S. Rangel², K. Ranjan²⁷, P.N. Ratoff⁴², P. Renkel⁷⁹, S. Reucroft⁶³, P. Rich⁴⁴, M. Rijssenbeek⁷², I. Ripp-Baudot¹⁸, F. Rizatdinova⁷⁶, S. Robinson⁴³, R.F. Rodrigues³, M. Rominsky⁷⁵, C. Royon¹⁷, P. Rubinov⁵⁰, R. Ruchti⁵⁵, G. Safronov³⁶, G. Sajot¹³, A. Sánchez-Hernández³², M.P. Sanders¹⁶, A. Santoro³, G. Savage⁵⁰, L. Sawyer⁶⁰, T. Scanlon⁴³, D. Schaile²⁴, R.D. Schamberger⁷², Y. Scheglov³⁹, H. Schellman⁵³, P. Schieferdecker²⁴, T. Schliephake²⁵, C. Schwanenberger⁴⁴, A. Schwartzman⁶⁸, R. Schwienhorst⁶⁵, J. Sekaric⁴⁹, S. Sengupta⁴⁹, H. Severini⁷⁵, E. Shabalina⁵¹, M. Shamim⁵⁹, V. Shary¹⁷, A.A. Shchukin³⁸, R.K. Shivpuri²⁷, D. Shpakov⁵⁰, V. Siccaldi¹⁸, V. Simak⁹, V. Sirotenko⁵⁰, P. Skubic⁷⁵, P. Slattey⁷¹, D. Smirnov⁵⁵, J. Snow⁷⁴, G.R. Snow⁶⁷, S. Snyder⁷³, S. Söldner-Rembold⁴⁴, L. Sonnenschein¹⁶, A. Sopczak⁴², M. Sosebee⁷⁸, K. Soustruznik⁸, M. Souza², B. Spurlock⁷⁸, J. Stark¹³, J. Steele⁶⁰, V. Stolin³⁶, D.A. Stoyanova³⁸, J. Strandberg⁶⁴, S. Strandberg⁴⁰, M.A. Strang⁶⁹, M. Strauss⁷⁵, E. Strauss⁷², R. Ströhmer²⁴, D. Strom⁵³, L. Stutte⁵⁰, S. Sumowidagdo⁴⁹, P. Svoisky⁵⁵, A. Sznajder³, M. Talby¹⁴, P. Tamburello⁴⁵, A. Tanasijczuk¹, W. Taylor⁵, J. Temple⁴⁵, B. Tiller²⁴, F. Tissandier¹², M. Titov¹⁷, V.V. Tokmenin³⁵, T. Toole⁶¹, I. Torchiani²², T. Trefzger²³, D. Tsybychev⁷², B. Tuchming¹⁷, C. Tully⁶⁸, P.M. Tuts⁷⁰, R. Unalan⁶⁵, S. Uvarov³⁹, L. Uvarov³⁹, S. Uzunyan⁵², B. Vachon⁵, P.J. van den Berg³³, R. Van Kooten⁵⁴, W.M. van Leeuwen³³, N. Varelas⁵¹, E.W. Varnes⁴⁵, I.A. Vasilyev³⁸, M. Vaupel²⁵, P. Verdier¹⁹, L.S. Vertogradov³⁵, M. Verzocchi⁵⁰, F. Villeneuve-Segulier⁴³, P. Vint⁴³, P. Vokac⁹, E. Von Toerne⁵⁹, M. Voutilainen^{67,e}, R. Wagner⁶⁸, H.D. Wahl⁴⁹, L. Wang⁶¹, M.H.L.S Wang⁵⁰, J. Warchol⁵⁵, G. Watts⁸², M. Wayne⁵⁵, M. Weber⁵⁰, G. Weber²³, A. Wenger^{22,f}, N. Wormes²¹, M. Wetstein⁶¹, A. White⁷⁸, D. Wicke²⁵, G.W. Wilson⁵⁸, S.J. Wimpenny⁴⁸, M. Wobisch⁶⁰, D.R. Wood⁶³, T.R. Wyatt⁴⁴, Y. Xie⁷⁷, S. Yacoub⁵³, R. Yamada⁵⁰, M. Yan⁶¹, T. Yasuda⁵⁰, Y.A. Yatsunenkov³⁵, K. Yip⁷³, H.D. Yoo⁷⁷, S.W. Youn⁵³, J. Yu⁷⁸, A. Zatserklyaniy⁵², C. Zeitnitz²⁵, D. Zhang⁵⁰, T. Zhao⁸², B. Zhou⁶⁴, J. Zhu⁷², M. Zielinski⁷¹, D. Zieminska⁵⁴, A. Zieminski⁵⁴, L. Zivkovic⁷⁰, V. Zutshi⁵², and E.G. Zverev³⁷

(The DØ Collaboration)

¹Universidad de Buenos Aires, Buenos Aires, Argentina

²LAFEX, Centro Brasileiro de Pesquisas Físicas, Rio de Janeiro, Brazil

³Universidade do Estado do Rio de Janeiro, Rio de Janeiro, Brazil

⁴Instituto de Física Teórica, Universidade Estadual Paulista, São Paulo, Brazil

⁵University of Alberta, Edmonton, Alberta, Canada,

Simon Fraser University, Burnaby, British Columbia,

Canada, York University, Toronto, Ontario, Canada,

and McGill University, Montreal, Quebec, Canada

⁶University of Science and Technology of China, Hefei, People's Republic of China

⁷Universidad de los Andes, Bogotá, Colombia

⁸Center for Particle Physics, Charles University, Prague, Czech Republic

⁹Czech Technical University, Prague, Czech Republic

¹⁰Center for Particle Physics, Institute of Physics,

Academy of Sciences of the Czech Republic, Prague, Czech Republic

¹¹Universidad San Francisco de Quito, Quito, Ecuador

¹²Laboratoire de Physique Corpusculaire, IN2P3-CNRS,

Université Blaise Pascal, Clermont-Ferrand, France

¹³Laboratoire de Physique Subatomique et de Cosmologie,

IN2P3-CNRS, Université de Grenoble 1, Grenoble, France

¹⁴CPPM, IN2P3-CNRS, Université de la Méditerranée, Marseille, France

¹⁵Laboratoire de l'Accélérateur Linéaire, IN2P3-CNRS et Université Paris-Sud, Orsay, France

¹⁶LPNHE, IN2P3-CNRS, Universités Paris VI and VII, Paris, France

¹⁷DAPNIA/Service de Physique des Particules, CEA, Saclay, France

¹⁸IPHC, Université Louis Pasteur et Université de Haute Alsace, CNRS, IN2P3, Strasbourg, France

¹⁹IPNL, Université Lyon 1, CNRS/IN2P3, Villeurbanne, France and Université de Lyon, Lyon, France

²⁰III. Physikalisches Institut A, RWTH Aachen, Aachen, Germany

²¹Physikalisches Institut, Universität Bonn, Bonn, Germany

²²Physikalisches Institut, Universität Freiburg, Freiburg, Germany

²³Institut für Physik, Universität Mainz, Mainz, Germany

²⁴Ludwig-Maximilians-Universität München, München, Germany

²⁵Fachbereich Physik, University of Wuppertal, Wuppertal, Germany

²⁶Panjab University, Chandigarh, India

²⁷Delhi University, Delhi, India

- ²⁸Tata Institute of Fundamental Research, Mumbai, India
²⁹University College Dublin, Dublin, Ireland
³⁰Korea Detector Laboratory, Korea University, Seoul, Korea
³¹SungKyunKwan University, Suwon, Korea
³²CINVESTAV, Mexico City, Mexico
³³FOM-Institute NIKHEF and University of Amsterdam/NIKHEF, Amsterdam, The Netherlands
³⁴Radboud University Nijmegen/NIKHEF, Nijmegen, The Netherlands
³⁵Joint Institute for Nuclear Research, Dubna, Russia
³⁶Institute for Theoretical and Experimental Physics, Moscow, Russia
³⁷Moscow State University, Moscow, Russia
³⁸Institute for High Energy Physics, Protvino, Russia
³⁹Petersburg Nuclear Physics Institute, St. Petersburg, Russia
⁴⁰Lund University, Lund, Sweden, Royal Institute of Technology and Stockholm University, Stockholm, Sweden, and Uppsala University, Uppsala, Sweden
⁴¹Physik Institut der Universität Zürich, Zürich, Switzerland
⁴²Lancaster University, Lancaster, United Kingdom
⁴³Imperial College, London, United Kingdom
⁴⁴University of Manchester, Manchester, United Kingdom
⁴⁵University of Arizona, Tucson, Arizona 85721, USA
⁴⁶Lawrence Berkeley National Laboratory and University of California, Berkeley, California 94720, USA
⁴⁷California State University, Fresno, California 93740, USA
⁴⁸University of California, Riverside, California 92521, USA
⁴⁹Florida State University, Tallahassee, Florida 32306, USA
⁵⁰Fermi National Accelerator Laboratory, Batavia, Illinois 60510, USA
⁵¹University of Illinois at Chicago, Chicago, Illinois 60607, USA
⁵²Northern Illinois University, DeKalb, Illinois 60115, USA
⁵³Northwestern University, Evanston, Illinois 60208, USA
⁵⁴Indiana University, Bloomington, Indiana 47405, USA
⁵⁵University of Notre Dame, Notre Dame, Indiana 46556, USA
⁵⁶Purdue University Calumet, Hammond, Indiana 46323, USA
⁵⁷Iowa State University, Ames, Iowa 50011, USA
⁵⁸University of Kansas, Lawrence, Kansas 66045, USA
⁵⁹Kansas State University, Manhattan, Kansas 66506, USA
⁶⁰Louisiana Tech University, Ruston, Louisiana 71272, USA
⁶¹University of Maryland, College Park, Maryland 20742, USA
⁶²Boston University, Boston, Massachusetts 02215, USA
⁶³Northeastern University, Boston, Massachusetts 02115, USA
⁶⁴University of Michigan, Ann Arbor, Michigan 48109, USA
⁶⁵Michigan State University, East Lansing, Michigan 48824, USA
⁶⁶University of Mississippi, University, Mississippi 38677, USA
⁶⁷University of Nebraska, Lincoln, Nebraska 68588, USA
⁶⁸Princeton University, Princeton, New Jersey 08544, USA
⁶⁹State University of New York, Buffalo, New York 14260, USA
⁷⁰Columbia University, New York, New York 10027, USA
⁷¹University of Rochester, Rochester, New York 14627, USA
⁷²State University of New York, Stony Brook, New York 11794, USA
⁷³Brookhaven National Laboratory, Upton, New York 11973, USA
⁷⁴Langston University, Langston, Oklahoma 73050, USA
⁷⁵University of Oklahoma, Norman, Oklahoma 73019, USA
⁷⁶Oklahoma State University, Stillwater, Oklahoma 74078, USA
⁷⁷Brown University, Providence, Rhode Island 02912, USA
⁷⁸University of Texas, Arlington, Texas 76019, USA
⁷⁹Southern Methodist University, Dallas, Texas 75275, USA
⁸⁰Rice University, Houston, Texas 77005, USA
⁸¹University of Virginia, Charlottesville, Virginia 22901, USA and
⁸²University of Washington, Seattle, Washington 98195, USA

(Dated: September 25, 2007)

We present a measurement of the muon charge asymmetry from W boson decays using 0.3 fb^{-1} of data collected at $\sqrt{s} = 1.96 \text{ GeV}$ between 2002 and 2004 with the D0 detector at the Fermilab Tevatron $p\bar{p}$ Collider. We compare our findings with expectations from next-to-leading-order calculations performed using the CTEQ6.1M and MRST04 NLO parton distribution functions. Our findings can be used to constrain future parton distribution function fits.

A measurement of the W^\pm boson rapidity (y_W) distributions in $p\bar{p}$ collisions provides valuable information about the parton distribution functions (PDFs) of the u and d quarks in the proton. W bosons at the Fermilab Tevatron $p\bar{p}$ Collider are primarily produced by quark-antiquark annihilation. Contributions from valence-valence and valence-sea annihilations provide about 85% of the cross section with the rest coming from sea-sea annihilations. A W^+ boson is usually produced by the interaction between a u quark from the proton and a \bar{d} quark from the antiproton, while a W^- boson is predominantly produced by a d quark from the proton and a \bar{u} quark from the antiproton. Since u valence quarks carry on average more of the momentum of the proton than d valence quarks [1, 2], W^+ bosons tend to move in the proton direction and W^- bosons in the antiproton direction, giving rise to the W boson production charge asymmetry.

The W^\pm boson production asymmetry provides complementary information on the PDFs to that from deep inelastic scattering experiments. In particular, it contributes to determining the slope of the d/u quark ratio in the region $x \lesssim 0.3$, where x is the momentum fraction carried by a parton in the proton [3, 4]. Knowledge of the d/u ratio is needed for predicting the transverse momentum (p_T) spectrum of leptons from W boson decay, an important ingredient in the precision measurement of the W boson mass.

The region of phase space in x that can be probed depends on the range of the rapidity of the W boson and, at leading order, is given by

$$x_{1(2)} = \frac{M_W \cdot c^2}{\sqrt{s}} e^{(\pm)y_W}, \quad (1)$$

where $x_{1(2)}$ is the momentum fraction carried by the $u(d)$ quark, $+(-)y_W$ is the rapidity of the positive (negative) W boson, and \sqrt{s} is the center of mass energy. For this analysis, $-2 \lesssim y_W \lesssim 2$ and $\sqrt{s} = 1.96$ GeV, allowing us to probe $0.005 \lesssim x \lesssim 0.3$.

The W boson rapidity is not directly measurable since the longitudinal momentum of the neutrino from its decay cannot be determined. However, the rapidity distribution of the charged lepton from the W boson decay reflects this asymmetry; here we use muons for this purpose. The muon asymmetry is a convolution of the W boson production asymmetry and the asymmetry from the $(V - A)$ nature of the W boson decay. Since the $(V - A)$ interaction is well understood, the muon charge asymmetry can be used to probe the PDFs.

The muon charge asymmetry as a function of the muon rapidity is defined as

$$A(y) = \frac{\frac{d\sigma}{dy}(\mu^+) - \frac{d\sigma}{dy}(\mu^-)}{\frac{d\sigma}{dy}(\mu^+) + \frac{d\sigma}{dy}(\mu^-)} \quad (2)$$

where $\frac{d\sigma}{dy}(\mu^\pm)$ is the differential cross section for the W^\pm boson decay muons as a function of muon rapidity y . In this analysis, we measure the muon charge asymmetry as a function of pseudorapidity $\eta = -\ln[\tan(\theta/2)]$, where θ is the polar angle with respect to the proton beam.

Allowing for acceptance and efficiency differences between positively and negatively charged muons, the muon charge asymmetry can be written as

$$A(\eta) = \frac{N_{\mu^+}(\eta) - k(\eta)N_{\mu^-}(\eta)}{N_{\mu^+}(\eta) + k(\eta)N_{\mu^-}(\eta)} \quad (3)$$

where η is the pseudorapidity of the muon, $N_{\mu^\pm}(\eta)$ is the background-corrected number of muons in pseudorapidity bin η , and $k(\eta) = \epsilon^+(\eta)/\epsilon^-(\eta)$ is the acceptance and efficiency ratio between the positive and negative muons.

The lepton charge asymmetry from W boson decay was measured by the CDF collaboration in the electron and muon channels during Run I of the Tevatron Collider [5, 6] and in the electron channel using Run II data [7]. The measurement described here is based on a larger data sample than these analyses used. In addition, the muon channel benefits from a much lower charge misidentification probability than the electron channel has.

For this analysis, we used 0.3 fb^{-1} of data collected using the D0 detector at a center-of-mass energy of 1.96 TeV at the Tevatron Collider. The D0 detector is described in detail in Ref. [8]; here we provide a brief description. The detector consists of a central tracking system, calorimeters, and a muon detector. The central tracking system comprises a silicon microstrip tracker (SMT) and a central fiber tracker (CFT), both located within a 2 T solenoidal magnet. The SMT has a six-barrel longitudinal structure interspersed with sixteen radial disks. The CFT has eight coaxial barrels, each supporting two doublets of overlapping scintillating fibers, measuring along the axial direction and at stereo angles of $\pm 3^\circ$. The liquid-argon/uranium calorimeter is in three sections, a central section covering $|\eta| \lesssim 1$ and two end caps extending coverage to $|\eta| \approx 4$. The calorimeter is surrounded by the muon detector which consists of three layers of scintillators and drift tubes, one layer in front of a 1.8 T iron toroidal magnet and two layers outside the magnet. Coverage for muons is partially compromised by the calorimeter support structure at the bottom of the detector ($|\eta| < 1.25$ and $4.25 < \phi < 5.15$, where ϕ is the azimuthal angle).

$W \rightarrow \mu\nu$ events were collected using two single-muon triggers. An unrescaled trigger, the ‘‘wide’’ trigger, covered the region $|\eta| < 1.5$, and a prescaled trigger, the ‘‘all’’ trigger, covered $|\eta| < 2$. Both triggers required hits in the muon system consistent in location and timing with a muon originating from the interaction region at the first trigger level, a reconstructed track in the muon system with $p_T > 3 \text{ GeV}/c$ at the second trigger level, and a track in the central tracking system with $p_T > 10$

GeV/ c at the third trigger level. Offline, muon candidates were required to lie within the geometrical acceptance of the detector, to have reconstructed track segments in at least two layers of the muon system, and to be matched to a track in the central tracking system with transverse momentum $p_T > 20$ GeV/ c . To ensure well-measured tracks, the matching track was required to have at least one hit in the SMT, at least nine hits in the CFT, a track fit $\chi^2/\text{dof} < 3.3$, and a distance of closest approach to the event vertex $|\text{dca}| < 0.011$ cm. Muon candidates were also required to be isolated in both the central tracking system and the calorimeter: the sum of the transverse momenta of the tracks in a cone of radius 0.5 in $\eta - \phi$ space around the muon track had to be less than 2.5 GeV/ c , and the total transverse energy in a hollow cone of inner radius 0.1 and outer radius 0.4 around the extrapolated muon position in the calorimeter had to be less than 2.5 GeV. Events with $|\eta| < 1.4$ ($1.4 < |\eta| < 2$) were required to satisfy the wide (all) trigger. W boson candidates were further selected by requiring the missing transverse energy \cancel{E}_T , determined by the vector sum of the transverse components of the energy deposited in the calorimeter and the p_T of the muon, to be greater than 20 GeV and the transverse mass $M_T > 40$ GeV/ c^2 . The analysis was done in muon pseudorapidity bins of width 0.2; each bin was treated independently. The pseudorapidity resolution of the tracking system is approximately 0.01 for $|\eta| < 1.7$ and is not expected to worsen significantly up to $|\eta| = 2$.

Events characteristic of the $Z \rightarrow \mu\mu$ background were removed using two criteria: (i) all events with a second muon were rejected, except those within $|\Delta\phi| < 0.1$ of the selected muon to avoid vetoing events containing multiple muons reconstructed from a single real muon at detector boundaries, and (ii) all events containing a second track with $|\Delta\phi| > 2.1$ from the selected muon, $p_T > 20$ GeV/ c , and $|\text{dca}| < 0.011$ cm were rejected. Cosmic ray muons were rejected using muon system scintillator timing cuts and by the dca requirement. A total of 189697 $W \rightarrow \mu\nu$ candidates was selected.

The asymmetry measurement is sensitive to the misidentification of the charge of the muon. A positive muon misidentified as a negative muon would not only add to the number of negative muons, but would also reduce the number of positive muons, and vice versa, diluting the true asymmetry. The charge misidentification probability was estimated using a dimuon data sample in which events were required to satisfy one of the two single-muon triggers described above. Events containing two muons satisfying all of the above conditions (except the second muon veto) and with a dimuon invariant mass $M_{\mu\mu} > 40$ GeV/ c^2 were selected to form a Z boson sample. The event sample contained 9958 events and only one same-sign dimuon event, giving an average charge misidentification probability of $(5.0^{+12}_{-4.2}) \times 10^{-5}$ over $-2 < \eta < 2$. Removing the dimuon invariant mass cut or lowering the muon p_T cut to 15 GeV/ c did not change the result. The probability was verified using an

independently-triggered dimuon sample in which events were collected using one of a set of dimuon triggers with no track requirements. Out of 19284 dimuon events selected as described above, two had same-sign muons. We also measured the probability using a sample of $W \rightarrow \mu\nu$ events generated with PYTHIA v6.2 [9] and CTEQ6.1M PDFs [10] and passed through the full D0 detector simulation based on GEANT [11]; it is approximately the same as that determined using the data. Therefore, charge misidentification is not expected to influence the final asymmetry measurement. To determine the systematic uncertainty on the asymmetry due to charge misidentification, we used Poisson uncertainties based on the number of muon tracks in each η bin from the single-muon-triggered Z boson sample and varied the asymmetry accordingly. The largest uncertainty due to charge misidentification is in the range $1.8 < \eta \leq 2.0$, where it is 0.001.

Ideally, the acceptances and efficiencies would be the same for all muons as a function of η and independent of charge and p_T , leading to $k(\eta) = 1$. To reduce charge effects due to detector asymmetries, the directions of the magnetic fields in the solenoidal and toroidal magnets were regularly reversed. Approximately 51.1% of the selected W boson sample was collected with the solenoid at forward polarity, with 48.9% at reverse polarity. For the toroid, 50.7% (49.3%) of the selected sample was collected with forward (reverse) toroid polarity, respectively. In addition, we studied the trigger efficiency for muons at the first two trigger levels, the trigger efficiency for tracks at the third trigger level, the offline muon reconstruction efficiency, the offline tracking efficiency, and the isolation efficiency. The four trigger and reconstruction efficiencies are discussed together while the isolation efficiency is discussed separately in the following text.

All efficiencies were measured using the tag and probe method on a sample of dimuon events collected using one of the single-muon triggers. To select primarily Z boson decays, events were required to have $M_{\mu\mu} > 40$ GeV/ c^2 . First a tag muon was chosen as a track-matched, isolated muon satisfying all of the selection conditions. The probe was another track or muon whose selection criteria depended on the efficiency being studied. All efficiencies were checked as functions of p_T , charge, and η . No dependence on p_T or charge was observed for the four trigger and reconstruction efficiencies. The four efficiencies were multiplied to determine the combined efficiencies for positive and negative muons as functions of η . Figure 1 shows the combined efficiencies by charge and the ratio of these efficiencies as functions of η . The ratio was fit to a constant value of 0.99 ± 0.01 , with a χ^2/dof of 0.71.

The isolation efficiency was also measured using the tag and probe method on a sample of dimuon events. One muon candidate was required to satisfy all muon and track selection requirements, while the other had to satisfy all requirements except that it was not required to be isolated in either the tracker or the calorimeter. The fraction of isolated probe tracks with $M_{\mu\mu} > 40$ GeV/ c^2 gives

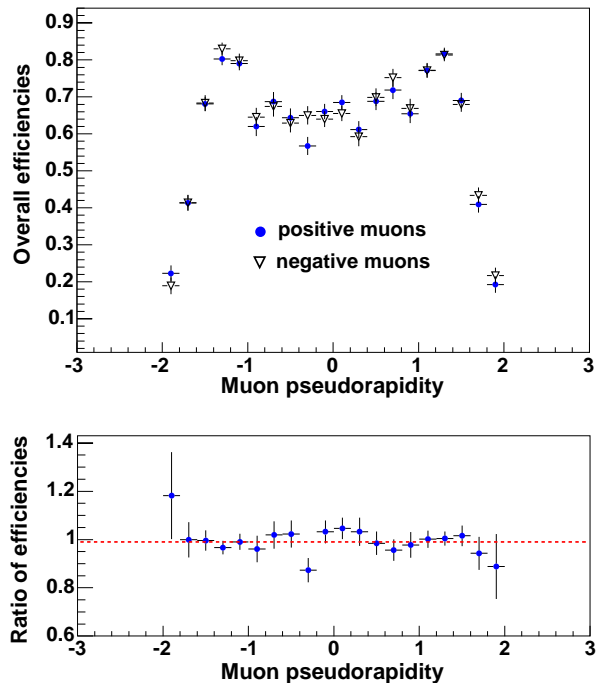


FIG. 1: (a) The combined trigger and reconstruction efficiency distributions by charge as a function of η and (b) the ratio of these efficiencies fit to a constant, 0.99 ± 0.01 .

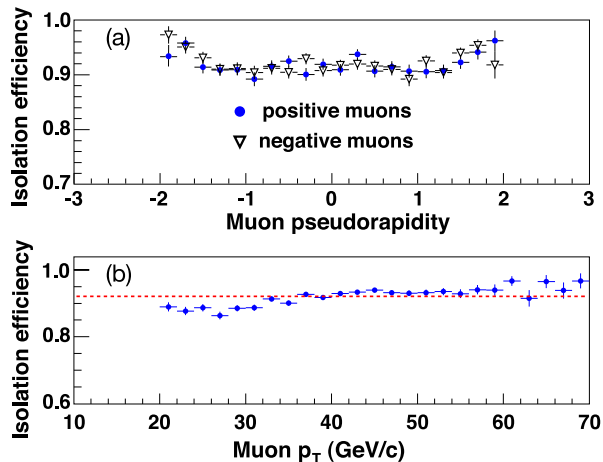


FIG. 2: The isolation efficiency as a function of (a) η (separated by muon charge) and (b) p_T (for all muons) fit to a constant 0.921 ± 0.002 .

the efficiency. The isolation efficiency is shown in Fig. 2 as a function of p_T and of η . The efficiency is constant for, and consistent between, both charges over the full η range. The efficiency as a function of p_T shows a slight p_T dependence. We chose, however, to fit the efficiency to a constant value of 0.921 ± 0.002 with a $\chi^2/\text{dof} = 5.8$. To account for the high χ^2/dof , the uncertainty was determined from the isolation efficiency distribution itself; the rms of this distribution is 0.022, and this value was used as the isolation efficiency uncertainty.

TABLE I: Estimated backgrounds in the W boson sample by trigger. Uncertainties are statistical only.

Background	Wide trigger	All trigger
$Z \rightarrow \mu\mu$	$(4.31 \pm 0.05)\%$	$(4.39 \pm 0.11)\%$
$Z \rightarrow \tau\tau$	$(0.19 \pm 0.01)\%$	$(0.20 \pm 0.02)\%$
$W \rightarrow \tau\nu$	$(2.32 \pm 0.02)\%$	$(2.43 \pm 0.08)\%$
Multijet events	$(2.77 \pm 0.04)\%$	$(2.76 \pm 0.09)\%$

The largest source of contamination in the data sample comes from electroweak processes, $Z \rightarrow \mu\mu$ and $W \rightarrow \tau\nu$ and $Z \rightarrow \tau\tau$ where $\tau \rightarrow \mu\nu$. Muons from these electroweak decays exhibit charge asymmetries which dilute the true asymmetry. These asymmetries are accounted for by subtracting the background bin-by-bin in η . The electroweak background was estimated using Monte Carlo samples generated with PYTHIA v6.2 and CTEQ6.1M PDFs and a parameterized description of the D0 detector [12]. For each of the three processes, separate samples were generated for the two triggers.

The background due to semi-leptonic decays and punch-through in multijet events was estimated using the data. The isolation criteria remove events containing muons within jets, and they were used as the discriminator to determine this background. Using a sample of events passing all selection criteria except that on the transverse mass and requiring $\cancel{E}_T < 10$ GeV, we measured the probability for multijet events to satisfy the isolation criteria. This probability shows no dependence on muon pseudorapidity.

Table I shows the overall contribution of each of the four backgrounds. To determine the number of events for each background, the contributions from the three electroweak processes were added to the number of events expected from $W \rightarrow \mu\nu$ Monte Carlo events produced using PYTHIA and the parameterized detector description, and this sum was normalized to the number of events in the data less the estimated multijet background. The overall normalization was done for $|\eta| < 1.5$ for the wide trigger and $|\eta| < 2$ for the all trigger, while for the final result, it was done independently in each η bin. This is the only use of signal Monte Carlo events in the analysis.

The muon charge asymmetry was determined separately for each bin in η and is shown in Fig. 3. Also shown are the asymmetry determined using the RESBOS [13] event generator with QCD resummation and PHOTOS [14] NLO QED corrections in the final state with the CTEQ6.1M PDFs, with the forty CTEQ6.1M PDF uncertainty sets [10, 15], and with the MRST04 NLO PDFs [16]. The next-to-next-to-leading-order calculation of the W boson rapidity distribution [17] at the Tevatron is very similar to the next-to-leading-order calculation. The W boson asymmetry distribution is not very sensitive to QCD corrections, and calculations at leading-, next-to-leading-, and next-to-next-to-leading-order are nearly indistinguishable [17].

Systematic uncertainties taken into account are those

TABLE II: The measured muon asymmetry in bins of pseudorapidity, calculated using Eq. 3. The asymmetry values are the averages within each pseudorapidity bin. The first uncertainty is statistical; the second is systematic.

Pseudorapidity range	Muon asymmetry
-2.0 – -1.8	$-0.096 \pm 0.089 \pm 0.005$
-1.8 – -1.6	$-0.020 \pm 0.036 \pm 0.005$
-1.6 – -1.4	$-0.103 \pm 0.024 \pm 0.005$
-1.4 – -1.2	$-0.140 \pm 0.009 \pm 0.005$
-1.2 – -1.0	$-0.138 \pm 0.011 \pm 0.005$
-1.0 – -0.8	$-0.120 \pm 0.012 \pm 0.005$
-0.8 – -0.6	$-0.132 \pm 0.011 \pm 0.005$
-0.6 – -0.4	$-0.090 \pm 0.011 \pm 0.005$
-0.4 – -0.2	$-0.049 \pm 0.011 \pm 0.005$
-0.2 – 0.0	$-0.011 \pm 0.010 \pm 0.005$
0.0 – 0.2	$0.028 \pm 0.011 \pm 0.005$
0.2 – 0.4	$0.050 \pm 0.011 \pm 0.005$
0.4 – 0.6	$0.071 \pm 0.011 \pm 0.005$
0.6 – 0.8	$0.120 \pm 0.011 \pm 0.005$
0.8 – 1.0	$0.122 \pm 0.012 \pm 0.005$
1.0 – 1.2	$0.127 \pm 0.011 \pm 0.005$
1.2 – 1.4	$0.107 \pm 0.009 \pm 0.005$
1.4 – 1.6	$0.065 \pm 0.025 \pm 0.007$
1.6 – 1.8	$0.042 \pm 0.036 \pm 0.005$
1.8 – 2.0	$-0.102 \pm 0.087 \pm 0.005$

on the ratio of the efficiencies for positively and negatively charged muons [$k(\eta)$], the efficiency of the isolation criteria, the charge misidentification, the probability for multijet events to satisfy the isolation criteria, the hadronic energy scale for the detector (needed to calculate \cancel{E}_T), and the parameterization of the muon energy loss in the calorimeter. Each contribution was varied by $\pm 1\sigma$, and the asymmetry was recalculated. The changes in the measured values were added in quadrature to determine the overall systematic uncertainty. The measured asymmetry and the statistical and systematic uncertainties are listed in Table II for each η bin. The efficiency ratio uncertainty, which is based on the number of dimuon events in the single-muon-triggered samples, dominates and is approximately equal to 0.005 in all η bins.

By CP invariance, the asymmetries at $\pm\eta$ have opposite signs and equal magnitudes, allowing the asymmetry distribution to be “folded” to decrease the statistical uncertainty. The folded asymmetry distribution was found by combining the numbers of events in each $\pm\eta$ bin and redetermining the background and systematic uncertainties as described above. The folded distribution is shown in Fig. 4 with the measured values of the asymmetry and uncertainties given in Table III. For $0.7 \lesssim |\eta| \lesssim 1.3$, our experimental uncertainties are smaller than the uncertainty given by the CTEQ uncertainty sets. Only at the extremes of our measurement, in the 0.0–0.2 and 1.8–2.0 muon pseudorapidity bins, are our uncertainties larger than the CTEQ uncertainty. Between these regions, the uncertainties are comparable.

We have measured the charge asymmetry of muons

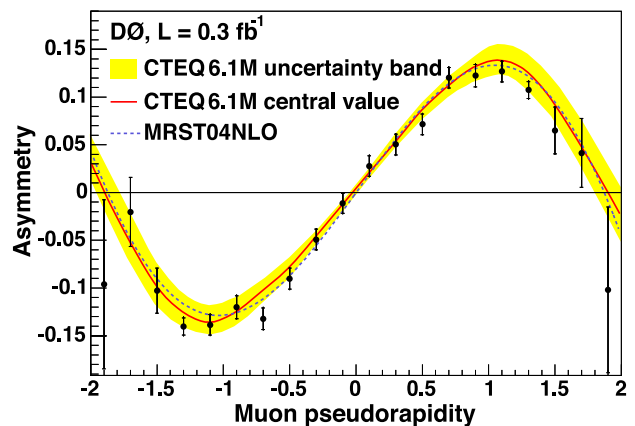


FIG. 3: The muon charge asymmetry distribution. The horizontal bars show the statistical uncertainty and the full vertical lines show the total uncertainty on each point. The shaded (yellow) band is the envelope determined using the forty CTEQ6.1M PDF uncertainty sets, the solid (red) line is the CTEQ6.1M central value, and the dotted (blue) line is the charge asymmetry determined using the MRST04 NLO PDFs. All three were determined using RESBOS and PHOTOS (color online).

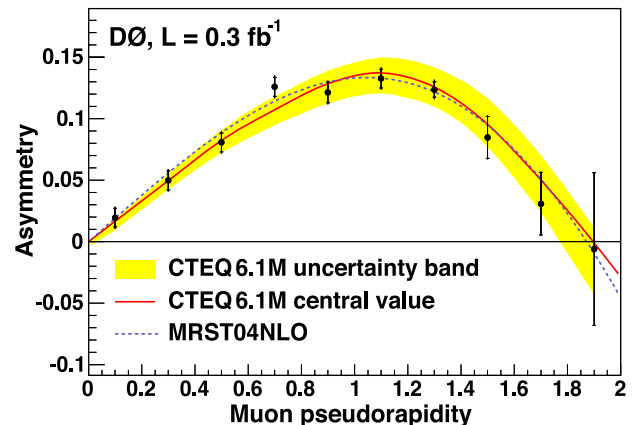


FIG. 4: The folded muon charge asymmetry distribution. The horizontal bars show the statistical uncertainty and the full vertical lines show the total uncertainty on each point. The shaded (yellow) band is the envelope determined using the forty CTEQ6.1M PDF uncertainty sets, the solid (red) line is the CTEQ6.1M central value, and the dotted (blue) line is the charge asymmetry determined using the MRST04 NLO PDFs. All three were determined using RESBOS and PHOTOS (color online).

from W boson decay using 0.3 fb^{-1} of data. Our results can already improve constraints on the PDFs. In the future, measurement of the W boson asymmetry will have a significant impact on PDF determination as present uncertainties are dominated by statistics.

We thank the staffs at Fermilab and collaborating institutions, and acknowledge support from the DOE and NSF (USA); CEA and CNRS/IN2P3 (France); FASI,

TABLE III: The folded muon asymmetry in bins of pseudorapidity. The asymmetry values are the averages within each pseudorapidity bin. The first uncertainty is statistical; the second is systematic.

Pseudorapidity range	Muon asymmetry
0.0 – 0.2	$0.019 \pm 0.008 \pm 0.005$
0.2 – 0.4	$0.050 \pm 0.008 \pm 0.005$
0.4 – 0.6	$0.081 \pm 0.008 \pm 0.005$
0.6 – 0.8	$0.126 \pm 0.008 \pm 0.005$
0.8 – 1.0	$0.121 \pm 0.008 \pm 0.005$
1.0 – 1.2	$0.133 \pm 0.008 \pm 0.005$
1.2 – 1.4	$0.124 \pm 0.006 \pm 0.005$
1.4 – 1.6	$0.085 \pm 0.017 \pm 0.006$
1.6 – 1.8	$0.031 \pm 0.026 \pm 0.005$
1.8 – 2.0	$-0.006 \pm 0.062 \pm 0.005$

Rosatom and RFBR (Russia); CAPES, CNPq, FAPERJ, FAPESP and FUNDUNESP (Brazil); DAE and DST (India); Colciencias (Colombia); CONACyT (Mexico); KRF and KOSEF (Korea); CONICET and UBACyT

(Argentina); FOM (The Netherlands); Science and Technology Facilities Council (United Kingdom); MSMT and GACR (Czech Republic); CRC Program, CFI, NSERC and WestGrid Project (Canada); BMBF and DFG (Germany); SFI (Ireland); The Swedish Research Council (Sweden); CAS and CNSF (China); Alexander von Humboldt Foundation; and the Marie Curie Program.

[a] Visitor from Augustana College, Sioux Falls, SD, USA.

[b] Visitor from The University of Liverpool, Liverpool, UK.

[c] Visitor from ICN-UNAM, Mexico City, Mexico.

[d] Visitor from II. Physikalisches Institut, Georg-August-University Göttingen, Germany.

[e] Visitor from Helsinki Institute of Physics, Helsinki, Finland.

[f] Visitor from Universität Zürich, Zürich, Switzerland.

[†] Fermilab International Fellow.

[‡] Deceased.

-
- [1] E. L. Berger, F. Halzen, C. S. Kim, and S. Willenbrock, *Phys. Rev. D* **40**, 83 (1989).
- [2] A. D. Martin, R. G. Roberts, and W. J. Stirling, *Mod. Phys. Lett. A* **4**, 1135 (1989).
- [3] H. L. Lai et al. (CTEQ Collaboration), *Phys. Rev. D* **51**, 4763 (1995).
- [4] S. Kuhlmann et al. (CTEQ Collaboration), *Phys. Lett. B* **476**, 291 (2000).
- [5] F. Abe et al. (CDF Collaboration), *Phys. Rev. Lett.* **74**, 850 (1995).
- [6] F. Abe et al. (CDF Collaboration), *Phys. Rev. Lett.* **81**, 5754 (1998).
- [7] D. Acosta et al. (CDF Collaboration), *Phys. Rev. D* **71**, 051104(R) (2005).
- [8] B. Abbott et al. (D0 Collaboration), *Nucl. Instrum. and Methods A* **565**, 463 (2006).
- [9] T. Sjöstrand et al., *Comput. Phys. Commun.* **135**, 238 (2001).
- [10] J. Pumplin et al. (CTEQ Collaboration), *J. High Energy Phys.* **07**, 012 (2002).
- [11] R. Brun and F. Carminati (1993), CERN Program Library Long Writeup W5013.
- [12] G. Hesketh, Ph.D. thesis, University of Manchester (2003), URL www-d0.fnal.gov/results/publications_talks/thesis/hesketh/thesis.ps.
- [13] C. Balazs and C.-P. Yuan, *Phys. Rev. D* **56**, 5558 (1997).
- [14] E. Barberio and Z. Was, *Comput. Phys. Commun.* **79**, 291 (1994).
- [15] D. Stump et al. (CTEQ Collaboration), *J. High Energy Phys.* **10**, 046 (2003).
- [16] A. D. Martin, R. G. Roberts, W. J. Stirling, and R. S. Thorne, *Phys. Lett. B* **604**, 61 (2004).
- [17] C. Anastasiou, L. Dixon, K. Melnikov, and F. Petriello, *Phys. Rev. D* **69**, 094008 (2004).